Combination of a Contactless Power Supply with an Electromagnetic Guiding for a Vertical Transportation System

R. Appunn, B. Riemer and K. Hameyer

Institute of Electrical Machines (IEM), RWTH Aachen University, Schinkelstr. 4, D-52056 Aachen, Germany
email: ruediger.appunn@iem.rwth-aachen.de

ABSTRACT

A contactless energy transmission system is essential to supply on-board systems of magnetic levitated vehicles without physical contact to a guiding rail. This paper introduces a combined contactless power supply (CPS) and electromagnetic guiding system (MGS). The actuator of the linear guiding system is part of an inductive energy transmission. With this approach two devices are integrated in one entity. The hybrid actuator consists of an omega shape iron yoke with permanent magnets and coils on its lateral arms. A primary winding is added to the elevator shaft and one of the MGS coils functions as secondary winding. Hereby a superposition of the MGS flux and the CPS flux emerges in the magnetic circuit of the actuator. A decoupling of the two systems is achieved by the high frequency of the CPS flux compared to the MGS flux. The proposed system requires less contruction space and weight compared to existing energy transmission systems.

1 INTRODUCTION

Contactless power transmission is of particular interest for electromagnetically levitated vehicles. The ability to transfer energy from a fixed guideway to the moving part without sliding contacts or traveling cables augments their benefits such as wearless operation. Electromagnetically levitated trains or other fast moving vehicles are able to consume power via harmonics induced by the propulsion device mounted to the guideway [1]. For slow vehicles, this concept is not suite, because an extra induction rail in the guideway and additional coils on the vehicle have to be constructed. This yields extra cost and requires additional construction space.

Previous studies to minimize both, cost and space, are based on an integrated solution of guiding and power transmission [2]. In this paper a similar strategy is followed. The MGS coil of an electromagnetic actuator, depicted in figure 1 functions as secondary winding for the energy transmission system. A further coil, consisting of one winding placed in two small slots on the guide rail produces a high frequent electromagnetic field, which superposes the levitating field. Hereby, a voltage is induced in the secondary coils mounted to the moving part and the power supply of the vehicle is established. Thereby, an integrated solution for both, contactless guiding and contactless power transmission using existing components is found. Figure 2 shows the topology.

The power transmission is designed to enhance the

Figure 1: Omega actuator without permanent magnets [3].

IEM elevator test bench in scale of 1:6. A nominal load of 200 W has to be transfered to supply the MGS coils and the on-board electronic components in the cabin such as eddy current sensors and current controllers.

2 COMPONENT MODELING

The general structure of the contactless power transmission system is presented in figure 3. Starting from a DC link an inverter topology generates a high frequent sinusoidal current. After primary reactive power compensation the transmission path i.e. the actuator entity is used. A secondary compensation follows hereafter. The voltage adjustment for the load is done by an active voltage control. The components of the CPS are described in detail in the corresponding sections.
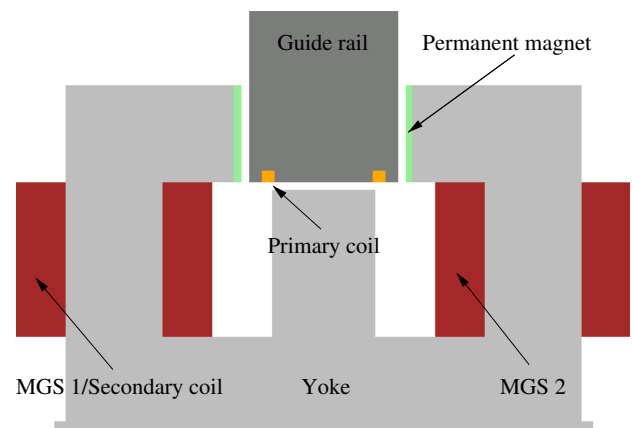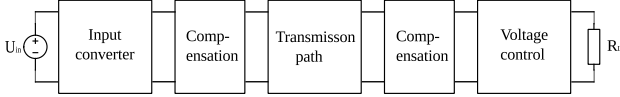

Figure 2: Omega actuator with CPS.

Figure 3: Components of the power transmission system.

2.1 Input converter

The inverter generates a high frequent alternating voltage from the DC link at the input of the circuit. The primary conductor is supplied with a load-independent, sinusoidal alternating current. This is essential for an efficient operation of the inductive power supply. The frequency of the energy transmission is chosen to be $f_0 = 10$ kHz. Hereby the trade-off between eddy current losses in the laminated steel and the permanent magnets of the actuator and an efficient power transmission will be realized. All resonant circuits are tuned to this frequency by

$$f_0 = \frac{1}{2\pi\sqrt{LC}}. \tag{1}$$

Figure 4 depicts the configuration of the input converter. A full bridge rectifier, consisting of four power MOSFETs or IGBTs is controlled by two rectangular signals with a phase shift of 180 degrees and the frequency f_0. A resonant circuit with the inductance L_{inv} and the capacitance C_{inv} enables a load independent current. To reduce interference currents which occur in reality, L_{inv} is separated symmetrically to the ground potential by two partial inductances [4]. With a system theoretical view to this configuration, a low pass is identified. Assuming a negligible series resistant of the inductance L_{inv}, the output current $I_p{}'$ is approximately load independent(Boucherot-circuit). At the output of the input inverter there is a transformer with a turn ratio of 10:1. Therefore the transfer ratio is $u = 10$. This transfer ratio is experienced to ensure the electrical insulation of the primary conductor and the input converter and to adjust the primary current I_p. Neglecting the resistance, the primary current can be written as

$$I_p = u \cdot I_p{}' = -u \cdot j \cdot \sqrt{\frac{C_{inv}}{L_{inv}}} \cdot U_{in}. \tag{2}$$

The output voltage of the inverter is rectangular shaped. The resulting harmonic components can be taken from figure 5. For an efficient power supply the primary current must be sinusoidal since the resonant circuits of the primary and secondary compensation are tuned to a fixed frequency. So spectral components of higher frequency cannot be utilized. The low pass characteristic of the LC-filter is determined by its quality factor. The quality factor
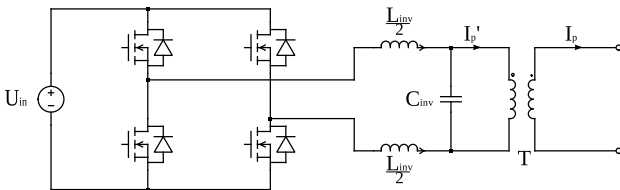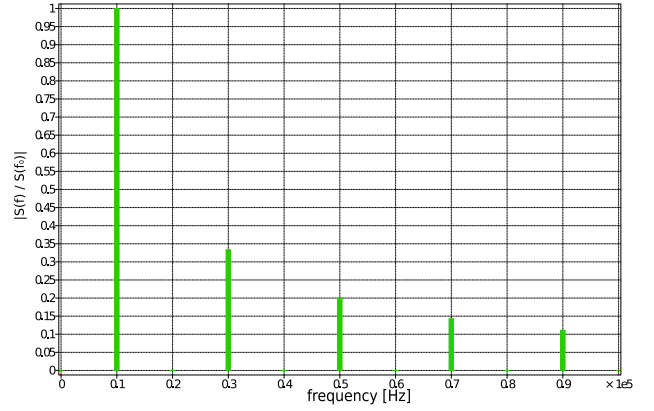

Figure 4: Input converter.

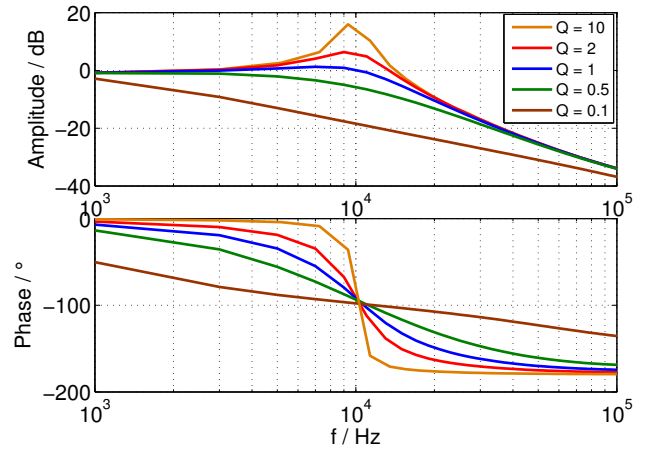Figure 5: Normalized amplitude spectrum of a rectangular signal of 10 kHz and duty cycle d=0.5.

Figure 6: Bode diagram of the LC filter.

for the aforementioned topology is defined as

$$Q = \frac{R'}{Z}. \tag{3}$$

R' is the total resistance of the circuit referenced to the primary side of the transformer, i.e. the sum of the reflected load resistance and all winding and conductor resistances. Z is the impedance of the resonant circuit, defined at resonance as

$$Z = \sqrt{\frac{L_{inv}}{C_{inv}}}. \tag{4}$$

Figure 6 depicts the frequency response of the LC filter in a Bode diagram as a function of the quality factor. To get a sinusoidal output current, the quality factor should be as high as possible. However, a high quality factor results in a bigger capacity C_{inv} when keeping the resonant frequency of the LC filter constant. Hereby the dynamic response of the system degrades. From simulation a quality factor of $Q \approx 1$ shows a sufficient damping of the third and fifth harmonic at $f = 30$ kHz and $f = 50$ kHz, without reducing the dynamic properties in an undesired dimension.

2.2 Transcription path

The contactless power transmission utilizes an electromagnetic flux created by the primary conductor, passing through the ferromagnetic yoke and guide rail, the permanent magnets and the air gaps. It induces an electromotive force in the secondary coils. In the studied scenario one MGS coil is used for energy transmission, only.

Theoretical framework Describing the transmission path as a transformer leads to the following differential equation system:

$$\begin{pmatrix} u_p \\ u_s \end{pmatrix} = \begin{pmatrix} R_p & 0 \\ 0 & R_s \end{pmatrix} \begin{pmatrix} i_p \\ i_s \end{pmatrix} + \partial_t \begin{pmatrix} \Psi_p \\ \Psi_s \end{pmatrix} \qquad (5)$$

with the winding resistances $R_{p,s}$. The time-derivative of the flux linkages is given by:

$$\partial_t \begin{pmatrix} \Psi_p \\ \Psi_s \end{pmatrix} = \partial_{\mathbf{i}} \begin{pmatrix} \Psi_p \\ \Psi_s \end{pmatrix} \cdot \partial_t \begin{pmatrix} i_p \\ i_s \end{pmatrix}. \qquad (6)$$

In the range of operation of the considered CPS system the ferromagnetic material is not saturated. Therefore the derivative $\partial_{\mathbf{i}}\mathbf{\Psi}$ is constant, this yields:

$$\partial_{\mathbf{i}} \begin{pmatrix} \Psi_p \\ \Psi_s \end{pmatrix} = \mathbf{L} = \begin{pmatrix} L_p & -M \\ -M & L_s \end{pmatrix}. \qquad (7)$$

$\mathbf{L}$ is the inductance matrix including all self and mutual inductances.

To determine the inductance matrix with an adequate accuracy to investigate the power transmission capability of the system, the matrix is extracted by means of the finite element method. The inductances are extracted as described in [5]. Because of the linear B-H characteristic in the range of operation the tangent inductance matrix is equal to the secant one [5]. To consider the different axial length of the long guide rail and the short omega actuator it is not sufficient to create a 2D FE model. Hence a 3D FE model of the actuator (figure 7) is generated. . Once the inductance matrix is extracted for the linear case all points of operation can be calculated analytically in the same accuracy as performed by a computational FE computation. A coupling of the FE model to the circuit simulator is not required. The inductance matrix of the considered actuator is given in table 1.

The magnetic coupling can be characterized by the coupling coefficient k,

$$k = \frac{M}{\sqrt{L_s \cdot L_p}}. \qquad (8)$$

In contrast to transformers, and due to the relativle large air gap, the coupling coefficient of contactless power supply systems is much smaller.

2.3 Compensation

Due to the inductances of primary and secondary windings the impedance of the transmission path has a significant inductive component. To avoid transmitting high reactive power and an oversized transformer T (figure 4), a
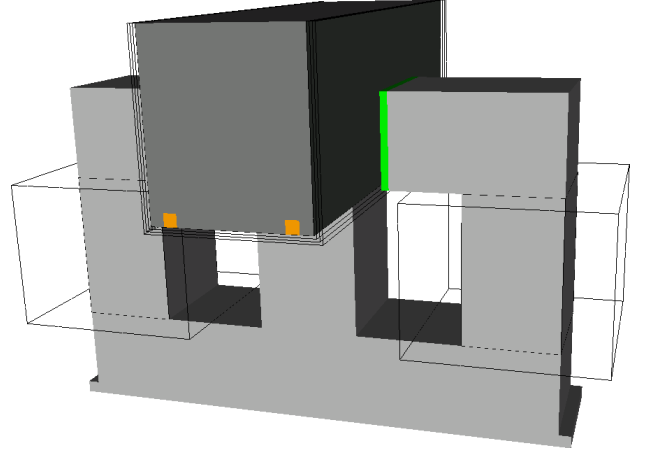

Figure 7: FE model of the actuator.

Table 1: Parameter of the inductance matrix describing the mutual inductors.

Inductance	Unit	
L_p	$[\mu H]$	2.77
L_s	$[mH]$	48.9
M	$[\mu H]$	65.7

power factor correction is required. Capacitances have to be added to the primary and the secondary circuit. Various topologies can be found in literature [6]. A series compensation on both sides (seriel-seriel-topology) is the most appropriate topology for the transmission path. In this case the secondary side has a voltage source characteristic and the reflected impedance has no imaginary part at resonance frequency. Herby the primary capacitance can be designed independently of the mutual inductance M and the coupling factor k respectively [7].

At resonant frequency ω_0 the reactances of a series resonance circuit are defined at

$$X = X_L + X_C = \omega_0 L - \frac{1}{\omega_0 C} = 0. \qquad (9)$$

With given inductances L_p and L_s, the required capacitances are

$$C_p = \frac{1}{L_p \cdot \omega_0{}^2}, \qquad (10)$$

$$C_s = \frac{1}{L_s \cdot \omega_0{}^2}. \qquad (11)$$

The quality factor of primary and secondary side are further important characteristics. For a series-series topology they are defined as

$$Q_p = \frac{L_p \cdot \omega_0}{Z_f} = \frac{L_p \cdot R_L}{M^2 \cdot \omega_0}, \qquad (12)$$

$$Q_s = \frac{L_s \cdot \omega_0}{R_L}. \qquad (13)$$

Here R_L is the load resistance at secondary side. Z_f is the transformed equivalent impedance of the secondary

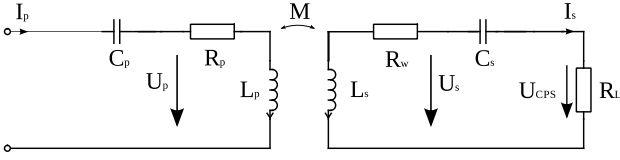$$Z_f = \frac{M^2 \cdot \omega_0{}^2}{R_L}. \qquad (14)$$

Figure 8: Equivalent circuit of the transmission path.

Figure 9: Output converter topology.

The ratio of Q_p and Q_s is an indicator for the system stability [8]. $Q_p \gg Q_s$ should be aspired. Whereas Q_s is already determined by the MGS coil on the actuator. With increasing length of the primary conductor Q_p is increasing, as well. The transmittable electric power can be calculated using the reflected impedance [7] defined in equation (14)

$$P_s = Re\{Z_f\} \cdot I_p^2 = I_p^2 \cdot \frac{M^2 \cdot {\omega_0}^2}{R_L}. \qquad (15)$$

With the equation of the secondary quality factor (13) we get

$$P_s = I_p^2 \cdot \frac{M^2 \cdot \omega_0 \cdot Q_s}{L_s}. \qquad (16)$$

The transmittable power depends quadratically on the primary current I_p and the mutual inductance M. A poor magnetic coupling can be compensated by a high primary current. The transmission path including load resistance and compensation is depicted in figure 8.

2.4 Output converter

Without further control the output voltage, supplying the load, is a high frequent sinusoidal alternating voltage at f_0. The amplitude is given at series secondary compensation by [6]

$$U_{CPS} = j\omega M I_p - I_s(j\omega L_s + \frac{1}{j\omega C_s} + R_w). \qquad (17)$$

At resonance frequency the reactances disappear, the output voltage is given by the following equation

$$U_{CPS} = j\omega M I_p - I_s R_w. \qquad (18)$$

The output voltage is load-variable. Therefore a voltage control has to be implemented. Moreover the contactless energy transmission system should supply a DC-link at 180 V, which is the basic voltage level for the electromagnetic guiding system. The output converter has to rectify the voltage and adjusts a fixed DC level. For filtering the voltage the existing DC-link capacitor can be utilized.

The open-source voltage ($I_s = 0$) of the power transmission system is directly proportional to the primary current I_p and therewith proportional to the input voltage U_{in}. To design an appropriate DC-DC converter, the range of the output voltage at a fixed primary current during nominal operation has to be known. In the examined topology the number of the secondary turns is much higher than the primary number of turns. This results in a high induced voltage on the secondary. To realize the required power transmission, the chosen primary current and voltage yield to a significantly higher output voltage U_{CPS} than 180 V.
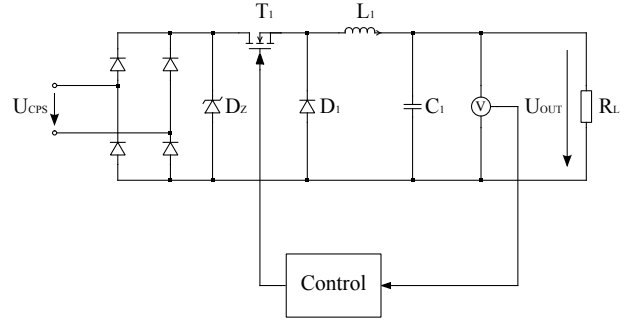
Therefore an buck converter is used to control the output voltage.

The topology of the output converter is depicted in figure 9. A diode rectifier rectifies the voltage U_{CPS}. Then U_{CPS} is stepped down using a buck converter consisting of the power MOSFET T_1, the diode D_1 and the inductance L_1. A detailed description of the step-down converter can be found in literature [9].

2.5 Output voltage control

The output voltage is controlled by transistor T_1. The DC-link voltage is measured and subtracted from a set-point value. This difference signal is used to generate a control signal for the gate drivers of the transistor. For comparison two different control strategies to operate the buck-converter are presented in the following paragraphs.

Hysteresis control Figure 10 presents the topology of the hysteresis control. The difference from the desired voltage and the DC-link voltage is given to a hysteresis element. The hysteresis defines the threshold of the deviation, when the control starts operation. The output voltage of the hysteresis element is connected to a comparator generating the control signal for the transistor. Using this control strategy the transistor is not operating at a fixed frequency. The load and the hysteresis value determine the operation frequency. Generally the frequency varies in a range of several 10 Hz.

The main advantage of this control strategy is its simple and robust design. The switching losses in transistor T_1 are marginal, since they are proportional to the low switching frequency. The relatively imprecise control of the output voltage is disadvantageous. During load condition a voltage ripple is detectable. At high load the voltage can
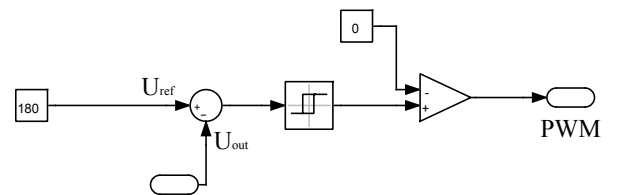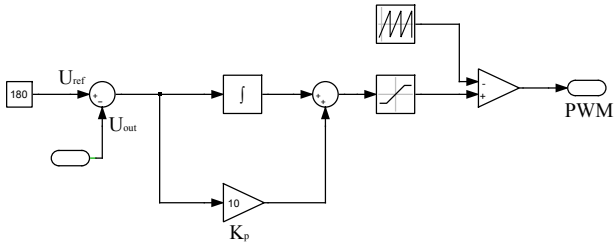

Figure 10: Hysteresis control.

Figure 11: PI controller.

Figure 12: Current density in a permanent magnet.

decline several percent. Wether this control strategy is applicable for a dynamic operation, resulting from the linear guiding systems influences, has to be studied.

PI Controller The PI controller scheme is depicted in figure 11. An additional anti-windup function resets the integrator when the signal reaches a threshold. Hereby the dynamic operation of the controller topology is improved. A comparison with a sawtooth signal of high frequency results in a pulse-width-modulated (PWM) signal. The duty cycle of the PWM regulates the output voltage of the inverter. This control strategy is more accurate than the hysteresis control. Load variations can be compensated much faster. However the complexity of the control is higher compared to the hysteresis control. Furthermore the switching losses increase since the switching frequency increases.

3 LOSSES

To determine the efficiency of the proposed inductive power transmission system a brief analysis of the different losses has to be done. Ohmic losses arise in the primary and secondary windings, whereas eddy current losses exist in the laminated steel of the actuator and the permanent magnets. Due to the offset magnetization of the iron circuit, resulting from the permanent magnets and the low amplitude of the magnetic flux density the hysteresis losses are neglected.

3.1 Coils

The power transmission is operating at 10 kHz, so skin and proximity effect has to be regarded when determining ohmic losses. To deal with this problem the primary conductor is built of high frequency litz wire. The secondary winding consists of standard copper wire as it is part of the MGS system. Depending on the actual material of the wire the losses are in a range of 20 W.

3.2 Laminations

Resulting from a high frequent alternating magnetic field, eddy current losses occur in the flux guiding parts of the actuator. Therefore the actuator and the part of the guide rail where the primary conductor is placed are fabricated of laminated steel. By finite element calculation the amplitude of the magnetic flux density B in actuator and guide rail is determined to be 0.02 Tesla. On an E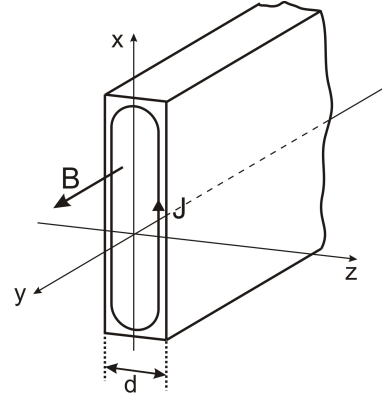pstein test frame a magnetic field of 10 kHz is applied to the laminations inducing the simulated flux density. Losses of $1.77 \frac{W}{kg}$ are measured.

3.3 Permanent magnets

The permanent magnet meterial on the lateral arms of the actuator is NdFeB. The conductivity of this rare earth material is not negligible. The eddy current losses in the magnets are calculated analytically [10]. Figure 12 defines the vectors of induction and current density and the geometrical parameters of the considered PM. The losses within the pm plate can be described with the following equation:

$$P = \frac{1}{24}\gamma \, \omega^2 d^2 B_m^2 V \frac{3}{kd} = \frac{\sqrt{2}}{8}\sqrt{\frac{\gamma\omega^3}{\mu}} dB_m^2 V. \quad (19)$$

Where γ is the electric conductivity, k the inverse skin depth, μ the permeability, B_m the mean magnetic flux density and V the volume of the plate. A reduction of the losses within the permanent magnet can be achieved by segmentation of the magnet plates. Using 10 plates with a length of $d = 5mm$ resulting in eddy current losses of 4.64 W.

4 SIMULATION RESULTS

Using the Piece-wise Linear Electric Circuit Simulation software PLECS [11], dynamic system simulation in Matlab/Simulink is performed. Hereby the control circuits can be described in a signal orientated environment, whereas the electrical quantities are described by equivalent circuits with concentrated parameters. Several load cases and the interaction with the magnetic guiding system is simulated. Figure 13 shows the output quantities i.e. voltage, current and output power, supplying the load resistance using the hysteresis control. Two load changes at 0.2 and 0.4 seconds are presented. The output voltage is controlled within the tolerance band. The simulated mean values of input and output power are presented in figure 14. Here a load change from 60 W to 190 W is shown. After a transient reaction resulting from the resonance circuits, a stable operation point is achieved. The load changes resemble the power demands of the coils, during operation of the MGS. It can be seen that the efficiency of the CPS
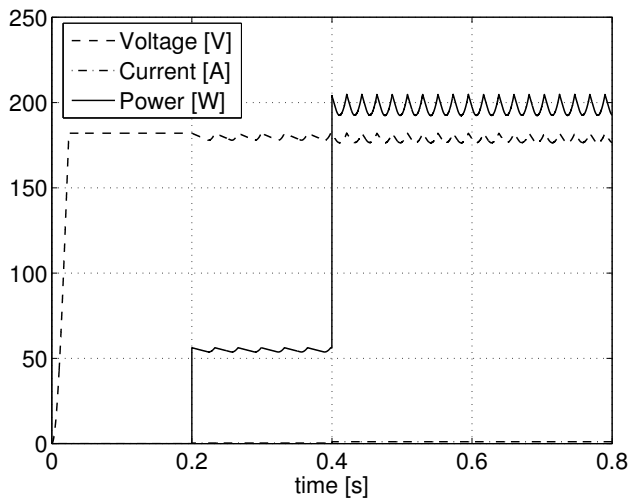
Figure 13: Output quantities of the contactless power transmission during load change.
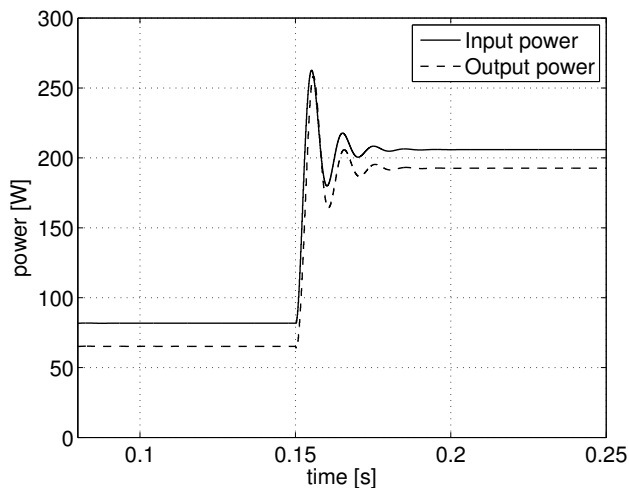

Figure 14: Input and output power during load change using PWM control.

is increasing, when getting closer to the nominal operation point at 200 W. Here only ohmic losses are regarded. The aforementioned eddy current losses, occurring in the laminations and permanent magnets, have to be added, resulting in an overall efficiency of $\sim 70\%$.

5   CONCLUSIONS

This paper focuses on a combined magnetic guiding system and contactless power supply actuator entity for a vertical transportation vehicle. The same flux path is used for both functions. Hereby construction space and costs can be reduced. The modeling of the inductive transmission path is done by concentrated parameters extracted from finite element analysis. A mutual inductance model is applied. A Boucherot circuit is proposed to generate a load independent input current of 10 kHz. Two control strategies for regulating the output voltage are presented. Results of dynamic system simulation of several load cases using the circuit simulator PLECS are shown. The interaction of the MGS and CPS is regarded and system stability is verified. First measurement resulting from an

Epstein test frame are presented to determine the losses in the iron laminations at the high transmission frequency. Ongoing research is done to include the contactless power transmission in an existing elevator test bench at the IEM institute. Measurement results of the interaction of the two principles will be presented in future work.

REFERENCES

[1] J.-Y. Lee, I.-J. Lee, J.-W. Kim, J.-H. Chang, D.-H. Kang, S.-U. Chung, and J.-P. Hong, "Contactless power transfer system combined with linear electric machine," in *Electrical Machines and Systems, 2007. ICEMS. International Conference on*, pp. 1544 –1548, 2007.

[2] B. Schmülling and K. Hameyer, "PowerTRACE - a Novel Power Transmission and Actuator Entity," in *20th International Conference on Magnetically Levitated Systems and Linear Drives, MAGLEV*, (San Diego, USA), pp. 15–18, December 2008.

[3] R. Appunn, B. Schmülling, and K. Hameyer, "Electromagnetic Guiding of Vertical Transportation Vehicles: Experimental Evaluation," *IEEE Trans. on Industrial Electronics*, vol. 57, pp. 335–343, January 2010.

[4] T. Wiesmann, "Von der Idee zum Produkt - Innovative Lösungen mit berührungsloser Energieübertragung in der Förder- und Sortiertechnik," in *Berührungslose Energieübertragung - Stand der Technik*, (Essen, Germany), Haus der Technik 2006, May 2006.

[5] E. Lange, F. Henrotte, and K. Hameyer, "An efficient field-circuit coupling based on a temporary linearization of fe electrical machine models," *Magnetics, IEEE Transactions on*, vol. 45, no. 3, pp. 1258 –1261, 2009.

[6] C.-S. Wang, O. Stielau, and G. Covic, "Design considerations for a contactless electric vehicle battery charger," *Industrial Electronics, IEEE Transactions on*, vol. 52, no. 5, pp. 1308 – 1314, 2005.

[7] C.-S. Wang, G. Covic, and O. Stielau, "Power transfer capability and bifurcation phenomena of loosely coupled inductive power transfer systems," *Industrial Electronics, IEEE Transactions on*, vol. 51, no. 1, pp. 148 – 157, 2004.

[8] J. Boys, G. Covic, and A. Green, "Stability and control of inductively coupled power transfer systems," *Electric Power Applications, IEE Proceedings -*, vol. 147, pp. 37 –43, January 2000.

[9] N. Mohan, T. M. Undeland, and W. P. Robbins, *Power Electronics - Converters, Applications and Design*. New York: John Wiley & Sons, 2003.

[10] K. Simonyi, *Theoretische Elektrotechnik*. Leipzig, Berlin, Heidelberg: Johann Ambrosius Barth, 1993.

[11] J. Allmeling and W. Hammer, "Plecs-piece-wise linear electrical circuit simulation for simulink," in *Power Electronics and Drive Systems, 1999. PEDS '99. Proceedings of the IEEE 1999 International Conference on*, 1999.